Applied Catalysis B: Environmental 165 (2015) 611–619

Contents lists available at ScienceDirect

Applied Catalysis B: Environmental

journal homepage: www.elsevier.com/locate/apcatb

Pt modified tungsten carbide as anode electrocatalyst for hydrogen oxidation in proton exchange membrane fuel cell: CO tolerance and stability

Ayaz Hassan, Valdecir Antonio Paganin, Edson Antonio Ticianelli*

Instituto de Química de São Carlos, Universidade de São Paulo, Caixa Postal 780, Fisico Quimica, Av. Trabalhador SaoCarlense, São Carlos CEP 13560-970, SP, Brazil

ARTICLE INFO

Article history:
Received 23 July 2014
Received in revised form
19 September 2014
Accepted 24 October 2014
Available online 31 October 2014

Keywords:
Carbon supported tungsten carbide
Hydrogen oxidation
CO tolerance
PEMFC

ABSTRACT

Pt supported on tungsten carbide-impregnated carbon (Pt/WC/C) is evaluated for hydrogen oxidation reaction in hydrogen/oxygen polymer electrolyte fuel cell at two different temperatures (85 and 105 °C), in absence and presence of 100 ppm CO. Carbon supported PtW, prepared by a formic acid reduction method is also evaluated for comparison. At 85 °C, the initial hydrogen oxidation activity in the presence of 100 ppm CO is higher for Pt/WC/C, showing a CO induced overpotential of 364 mV for 1 A cm^{-2} of current density as compared to an overpotential of 398 mV for PtW/C. As expected, an increase in CO tolerance is observed with the increase in cell temperature for both the catalysts. The increased CO tolerance of Pt/WC/C catalyst is in agreement with CO stripping experiments, for which the CO oxidation potentials occurred at lower potentials at three different temperatures (25, 85 and 105 °C) in comparison to PtW/C. The stability of both electrocatalysts is evaluated by an accelerated stress test and the results show a better stability for Pt/WC/C catalyst. On the basis of cyclic voltammograms and polarization curves, it is concluded that Pt/WC/C is more stable than PtW/C and can be used as alternative anode catalyst in PEMFC, especially at high temperatures.

1. Introduction

In recent years, proton exchange membrane fuel cells (PEMFCs) have been recognized as the most feasible power source for low/zero-emission electric vehicles and stationary applications [1]. In such type of fuel cells, H_2 is used as fuel and O_2/air as oxidant [2]. Utilization of pure hydrogen as fuel is the simplest and most efficient way for PEMFCs, but the infrastructure required is limited due to the production cost and storage difficulties. Alternatively, hydrogen may be obtained from reformed fuels, such as steam-reformed methanol, ethanol or natural gas. A potential problem which arises from this system is the production of small amount of impurities particularly carbon monoxide, which strongly adsorb on the Pt catalyst, usually employed in the anode [3], blocking the sites for the hydrogen adsorption and oxidation. Therefore, Pt is modified with other elements such as Ru or Mo for the PEMFCs so as to search for enhanced CO tolerant materials [4,5]. Unfortunately, the relative high cost and insufficient durability of these elements still hinder the large scale commercialization of PEMFCs. For example, Antolini [6] observed the dissolution of Ru from the Pt–Ru anode catalyst and its presence in the cathode side. Other studies have shown the dissolution of Mo from the Pt–Mo anode and its transfer through the electrolyte membrane to the cathode side [7,8]. Therefore, most robust materials are required to provide not only stability to the anode catalysts, but also ability to tolerate trace amounts of CO. Because the catalytic properties of transition metal carbides have been found to be similar to those of precious metals like Pt [9], extensive studies have been carried out using transition metal carbides, particularly WC, as catalyst supports to improve the catalytic performance and minimize usage of precious metals. As electrocatalysts, they are also known to be highly resistant to CO poisoning and stable in acidic and basic solutions [10]. This is most probably due to the active surface of WC toward the dissociation of H_2O to produce surface hydroxyl group [11], which are critical for the subsequent oxidation of CO. If used as support, WC helps to increase the dispersion of precious metals [12].

There have been recent studies to evaluate the use of tungsten carbide as catalyst for fuel cells and it has been shown that Pt supported on tungsten carbide presents superior activity for both, the methanol electro-oxidation and oxygen reduction

* Corresponding author. Tel.: +55 16 3373 9945; fax: +55 16 3373 9952.
E-mail address: edsont@iqsc.usp.br (E.A. Ticianelli).

http://dx.doi.org/10.1016/j.apcatb.2014.10.068
0926-3373/

reactions [13,14]. In the work performed by Chhina et al. [15] a higher activity and stability for oxygen reduction reaction before and after 100 oxidation cycles was shown by the Pt/WC as compared to Pt/C. In another study, it has been observed that Pt supported on tungsten carbide shows higher activity for electrochemical oxidation of methanol than a commercial carbon supported PtRu electrocatalyst [16]. Lee et al. [17] reported that Pd/WC shows improved activity for the electro-oxidation of methanol as compared to a Pd/C catalyst in an alkaline media. Similarly, in the work conducted by Moon and co-workers [18], it has been demonstrated that Pd supported on mesoporous tungsten carbide showed a more negative peak potential compared to Pd/C in the CVs for methanol electrooxidation. They also evaluated the stability of these electrocatalysts in alkaline solution containing methanol and reported only 2.2% decrease in current density for Pd/meso-WC after stability test compared to a decrease of 26% for Pd/C. In a subsequent study, it has been shown that tungsten carbide alone has low activity for the methanol and hydrogen oxidations [19]. The hydrogen oxidation activity of WC-based anode in absence of noble metals was also evaluated by Yanga and Wang [20]. They observed that WC has very low activity toward hydrogen oxidation. However, the activity could be improved significantly by adding a small amount of Pt to tungsten carbide [21,22]. Hence, in the work performed by Ham and co-workers, the Pt/WC catalyst showed two times higher activity per mass of Pt for hydrogen oxidation compared to a commercial Pt/C [23].

Similarly, Kelly et al. [24] investigated the hydrogen evolution activity of Pd supported on tungsten and molybdenum carbide. In their work a superior activity was noted for Pd/C in contrast to bare carbides. Nevertheless, only the addition of monolayer of Pd to these carbides doubled the values of corresponding current density for the resultant carbide based electrocatalysts. Furthermore, the activity and stability of Pt supported on tungsten carbide has been tested for hydrogen evolution and oxidation reaction by Liu and Mustain [25]. Although they found a very little difference in the activity of Pt/WC and Pt/C catalysts for hydrogen evolution reaction, the stability of Pt/WC was far better than that of Pt/C. A loss of only 4% in activity was observed for Pt/WC which was very small in comparison to loss in activity of more than 20% for Pt/C.

Summarizing, there has been some research data in the literature on the use of tungsten carbide as anode materials, either for hydrogen oxidation/evolution or for methanol oxidation. However, the CO tolerance and stability of this material as anode electrocatalyst in a real fuel cell environment has not been studied in detail. Thus in this work, carbon supported tungsten carbide prepared by a simple impregnation method was used as Pt catalyst supports in the anode of a PEMFC. The Pt was supported on this carbide by a formic acid reduction method. The resulting catalyst was first tested for hydrogen oxidation in the presence of pure hydrogen and hydrogen containing CO and then its stability was evaluated by an accelerated stress test [26], applying an electrode potential cycling, from a low to a high potential. The results obtained were compared with carbon supported PtW catalyst, which was also prepared by formic acid reduction method.

2. Experimental

2.1. Electrocatalysts preparation

Tungsten carbide supports with different W/C wt. percentages (10, 20 and 30) were prepared by a simple impregnation method [27]. Briefly, the tungsten precursor (WCl_6, Aldrich) and carbon black (Vulcan XC-72) were added in to ethanol and then the composite was impregnated for 3 h at room temperature. The mixture was then heated at 70 °C, until the ethanol was evaporated completely. The resultant solid was transferred in to a quartz reactor, placed in a tubular furnace and heat treated under CH_4/H_2 atmosphere at 800 °C for 3 h to give the tungsten carbide, which was passivated using a 1% O_2/Ar mixture for atleast 3 h, prior it was taken outside the quartz reactor. Pt (20 wt.%) was deposited on these carbide supports by the formic acid reduction method, which consisted of the reduction of dihydrogen hexachloroplatinate hexahydrate ($H_2PtCl_6{\cdot}6H_2O$, Aldrich), in the presence of the prepared tungsten carbide, using formic acid as reducing agent [7,8,28]. These catalysts were then designated as Pt/WC/C10, Pt/WC/C20 and Pt/WC/C30, where the numbers represent the W/C wt.% ratios. For the purpose of comparison, PtW/C (60:40 atomic proportions) was prepared by the same formic acid method, maintaining the metal content at 20 wt.%. Pt supported on Vulcan XC-72 carbon also with 20 wt.% metal/C was supplied by E-TEK. The Pt and PtW loading in all electrocatalysts was maintained at 20 wt.%.

2.2. Physical characterizations

The real tungsten content of the WC/C supports, as well as the metal loadings (Pt and W) of the catalysts were estimated by energy dispersive x-ray spectroscopy (EDX) in a scanning electron microscope LEO, 440 SEM-EDX system (Leica-Zeiss, DSM-960) with a microanalyzer (Link analytical QX 2000) and a Si (Li) detector, using a 20 keV incident electron beam. X-ray diffraction (XRD) analyses of the materials were conducted using a RIGAKU XRD RU200B diffractometer (Cu K_α radiation), in the 2θ range from 10 to 90°. X-ray photoelectron spectroscopy (XPS) measurements were conducted for the investigation of surface oxidation state of the catalysts. XPS studies were conducted at the National Synchrotron Light Laboratory (LNLS) on a SPECS (spectrometer-Phoibos HSA3500 MCD9 150) equipped with a InSb (1 1 1) monochromator and X-rays with energy of 1840 eV. The energy was calibrated to give a binding energy of 84 eV for the gold 4f 7/2 region. The instrument was programmed for the passage of 20 eV energy, with the energy step of 0.1 eV and acquisition time of 200 ms. Particle size distributions of Pt and PtW nanoparticles were determined by transmission electron microscopy (TEM, JEOL 2100 transmission electron microscope). The average crystallite sizes of Pt in the catalysts were determined by the Scherrer equation [29], using the Pt (2 2 0) diffraction peak and were compared with the results from TEM.

2.3. Electrochemical measurements

The electrochemical measurements were conducted in a single cell, using membrane electrode assemblies (MEAs) prepared with Nafion 115 membranes (DuPont, USA) in the middle and electrodes formed by gas diffusion and catalyst layers on both sides of the membrane. The method of preparation of MEAs can be found in literature [30]. Fuel cell polarization measurements were carried out galvanostatically with the cell at two different temperatures (85 and 105 °C). For 85 °C the gases were saturated with water at 100 °C and 2 atm for the anode and at 90 °C and 1.7 atm for the cathode, whereas at 105 °C the gases were saturated at 120 °C and 3 atm for the anode and 110 °C and 2.7 atm for the cathode. The system was first maintained at an initial potential of 0.7 V in pure H_2, for 2 h, and then at 0.8 V in H_2/100 ppm CO, also for 2 h, to reach the steady state before the data acquisition at both the temperatures. In these experiments the cathode was constantly fed with O_2. *On line* mass spectrometry (Pfeiffer Vaccum GSD 301 Omnistar, quadrupole QMS 200 Prisma, W filament 70 eV electron energy with SEM 1000 V common voltage) measurements at the anode outlet was used to monitor the formation of CO_2 as a function of the cell potential. In these experiments the anode was fed with either H_2 or H_2/100 ppm CO, whereas the cathode was constantly fed with O_2, keeping the cell at the condition of open circuit potential.

Cyclic voltammetries of the anodes were conducted using a Solartron 1285 potentiostat/galvanostat in the standard fuel cell hardware. During experiments the anode, used as working electrode, was fed with Ar, while the cathode, used as both reference (reversible hydrogen electrode, RHE corrected approximately to 35 mV) and counter electrode was constantly fed with H_2. CO stripping experiments were conducted at three different temperatures (25, 85 and 105 °C), in order to evaluate the CO oxidation ability of the anode materials. These experiments were conducted in a similar way as for the cyclic voltammetry, except that the anode was either fed with Ar or CO (1000 ppm in Ar balance). The CO was firstly adsorbed on the anode for 30 min at a constant potential of 100 mV for 25 °C and at 50 mV for 85 and 105 °C, and then the anode was flushed with Ar for another 30 min. OLMS analyses were performed to know about the oxidation of the adsorbed CO on the surface of electrocatalysts.

The effect of voltage cycling on the single cell electrodes was investigated by applying cycling voltammetry as a degradation inducing technique, in the same set up and conditions described above. The anode potential was scanned between 0.1 and 0.7 V, at a scan rate of 50 mV s^{-1}, at room temperature, up to a total of 5000 cycles. The MEAs performance was evaluated first with freshly prepared electrodes then after 1000, 3000 and finally after 5000 potential cycles by measuring polarization curves and anode overpotentials due to the presence of CO (η_{CO}). These anode overpotentials were calculated as $\eta_{CO} = E_{H_2} - E_{H_2/CO}$, where E_{H_2} and $E_{H_2/CO}$ are the cell potentials in the absence and presence of CO (i.e., with the anode fed with pure H_2 and H_2 + 100 ppm CO, respectively). Cyclic voltammetry of the Pt/C cathodes was conducted in the same way as for the anodes, after the polarization measurements and the voltage cycling processes.

3. Results and discussions

3.1. Physical characterization of the electrocatalysts

The wt.% of the different components of the catalysts as obtained by EDX are given in Table 1. The tungsten contents in the tungsten carbide supports are less than the target values of 10, 20 and 30 wt.% and this was also observed for the Pt loading of the Pt/WC/C, whereas the wt.% of PtW/C is very close to the desired value, with a Pt:W atomic ratio quite closed to the expected value (3:2). In all cases, the ranges of the catalyst contents were considered satisfactory for the purpose of the present investigation.

The XRD results of the prepared materials are presented in Fig. 1. The XRD patterns of WC/C supports correspond to those of simple hexagonal planes of WC according to JCPDF 65-8828. As can be observed, the intensities of peaks in the XRD patterns of tungsten carbide supports increase in the order of WC/C10 < WC/C20 < WC/C30, which are consistent to EDX analysis, where the percentage of W in the supports increases in the same order as mentioned above. The peak at ca. 25° corresponds to the 0 0 2 crystal plane of hexagonal structure of Vulcan XC-72 carbon, which confirmed the existence of tungsten carbide supported on carbon. From the intensities of carbon peaks in these

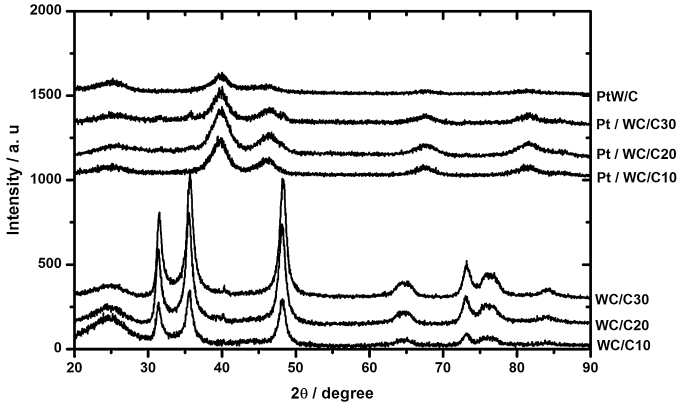

Fig. 1. X-ray diffraction patterns of WC/C supports and Pt/WC/C10, Pt/WC/C20, Pt/WC/C30 and PtW/C electrocatalysts.

XRD patterns, it is confirmed that the WC/C10 contains the highest amount of carbon, whereas the WC/C30 contains least amount, as also determined by EDX.

The diffraction patterns of Pt/WC/C10, Pt/WC/C20, Pt/WC/C30 and PtW/C exhibit major peaks of face centered cubic crystalline structure of Pt, corresponding to 1 1 1, 2 0 0, 2 2 0 and 3 1 1 crystal planes, besides weaker reflections of WC at 32°, 36° and 48° in the XRD pattern of Pt/WC/C20 and Pt/WC/C30. For Pt/WC10 the WC peaks didn't appear because of small amount of W present. Fig. 2 shows the XPS spectra for the PtW/C catalyst in the Pt 4f and W 4f regions. As can be observed in Fig. 2a, three pairs of doublets are found in the Pt 4f regions, which can be assigned to Pt(0), PtO(II) and PtO_2(IV) species. The binding energy of these species are located at 71.24, 74.54 eV; 72.06, 75.36 eV and 73.48, 76.78 eV. The binding energies corresponding to first set of doublet (Pt $4f_{7/2}$ and Pt $4f_{5/2}$ of Pt (0)) are exactly the same as of pure Pt nanoparticles. This means that W is not alloyed with Pt in PtW/C catalyst, as also evidenced by XRD analysis. Fig. 2b shows the XPS spectra in the W 4f region, where the first doublet at 35.67 and 37.82 eV can be assigned to WO_3 and the second doublet at 35.01 and 37.19 can be attributed to WO_2. This indicates that W in the PtW/C is mostly present in the oxides form.

TEM images of Pt/WC/C20 and PtW/C shown in Fig. 3, exhibit quite uniform dispersion of Pt and PtW nanoparticles. The Pt particles supported on WC/C are more evenly distributed than the PtW on carbon black, which suggests that the carbide phase facilitates the dispersion of particles. In the insets of Fig. 3 are shown the histograms for both the catalysts, which are based on the analysis and counting of 200 particles from several different regions of the same catalyst. As can be observed from the two histograms, the particle size distribution is quite uniform for both the catalysts. Results of crystallite sizes obtained from XRD and mean particle sizes obtained by TEM are included in Table 1. A good correlation can be seen for these results, regarding crystallite and particle sizes. The particle size of PtW in PtW/C catalyst is compatible with the particle size of Pt in Pt/WC/C20 catalyst, although in the latter case the average size is somewhat larger.

Table 1
Chemical compositions, crystallite/particle sizes and molar ratio of WC/C supports and the Pt/WC/C20 and PtW/C electrocatalysts.

Electrocatalysts	Element (wt.%) determined by EDX			Pt crystallite/particle size (nm)			EDX molar ratio
	Pt (%)	W (%)	C (%)	XRD	TEM	TEM after testing	
WC/C10	NA	8.7	91.3	NA	NA	NA	NA
WC/C20	NA	15.0	85.0	NA	NA	NA	NA
WC/C30	NA	19.3	80.7	NA	NA	NA	NA
Pt/WC/C20	16.9	12.5	70.6	2.4	3.6	3.6	NA
PtW/C	11.8	7.2	81.0	2.3	2.3	2.6	3.2:1.8

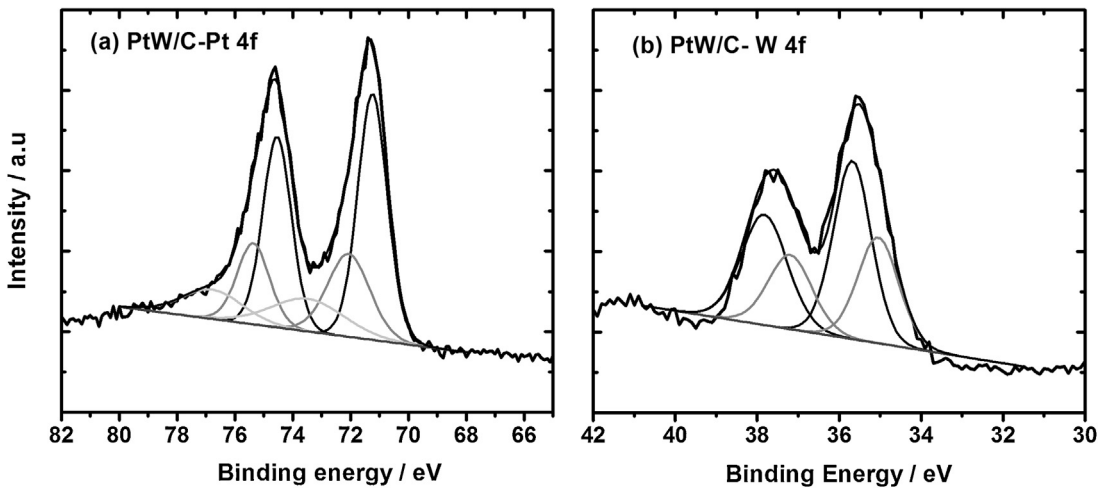

Fig. 2. XPS spectra of PtW/C catalyst. (a) Pt 4f region and (b) W 4f region.

3.2. Electrochemical results

Fig. 4 shows polarization curves obtained for the single cell anodes with Pt/WC/C10, Pt/WC/C20 and Pt/WC/C30, supplied with H_2 and H_2 containing 100 ppm CO, and cathodes (Pt/C), supplied with O_2. These polarization curves were recorded initially with freshly prepared electrodes and then after 1000, 3000 and 5000 potential cycles. As expected, the cell performance drops significantly when the H_2 containing CO is introduced to the anode. The highest initial (0 cycle) hydrogen oxidation activity in the presence of CO is observed for Pt/WC/C10 (Fig. 3a) which gave CO induced overpotential (η_{CO}) of 288 mV for 1 A cm^{-2} of current density as compared to overpotentials of 364 and 378 mV for Pt/WC/C20 (Fig. 3b) and Pt/WC/C30 (Fig. 3c), respectively. Nevertheless, for PtWC/C10 the cell voltage dropped more drastically with the cycling process, in the presence of both H_2 and H_2 containing CO, which is also confirmed by greater decrease of the current density in the cyclic voltammograms with the cycling process for this catalyst, shown in the Fig. S1 of Supporting material. This is an evidence that an increase in the amount of carbide, imparts stability to the catalyst. Since Pt/WC/C20 showed a good stability and intermediate CO tolerance, further study was continued only with this catalyst and compared to PtW/C.

Fig. 5 shows a comparison of the cell voltages for the Pt/WC/C20, PtW/C and Pt/C electorocatlysts in the presence and absence of CO, at two different temperatures. At 85 °C (Fig. 5a) better cell performance in the presence of CO is observed for Pt/WC/C20, which showed a CO induced overpotential (η_{CO}) of ca. 364 mV for 1 A cm^{-2} of current density, as compared to an overpotential of 398 mV for the PtW/C catalyst. On the other hand for Pt/C the effect of CO poisoning is so adverse that the current density hardly reached 1 A cm^{-2}. Such a high ovepotentials can't be tolerated in the fuel cell operating practically. At a higher temperature (105 °C) also, the Pt/WC/C20 showed a better CO tolerance in comparison to PtW/C. In this case, the anode overpotential values obtained were 104 and 174 mV at 1 A cm^{-2} of current density for Pt/WC/C20 and PtW/C, respectively. Here the CO tolerance of Pt/C is comparable to that of PtW/C, showing the impact of increase in temperature on the CO tolerance.

The CO tolerance mechanism of Pt–W catalysts has been studied in detail in literature [31,32]. It has been proposed that enhanced CO tolerance of these materials compared to Pt alone is due to the change in the oxidation state of W, occurring at low electrode potential which renders the tungsten sites to be active for the dissociative adsorption of water and thus to the oxidation of adsorbed CO on Pt. Nevertheless, in the case of Pt/WC/C20 there may have

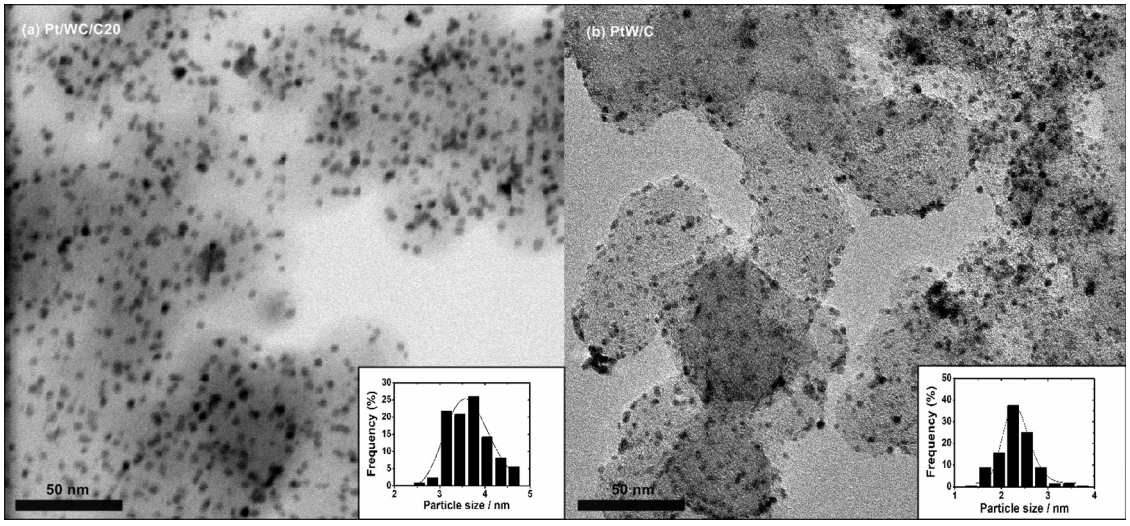

Fig. 3. TEM images of Pt/WC/C20 and PtW/C electrocatalysts.

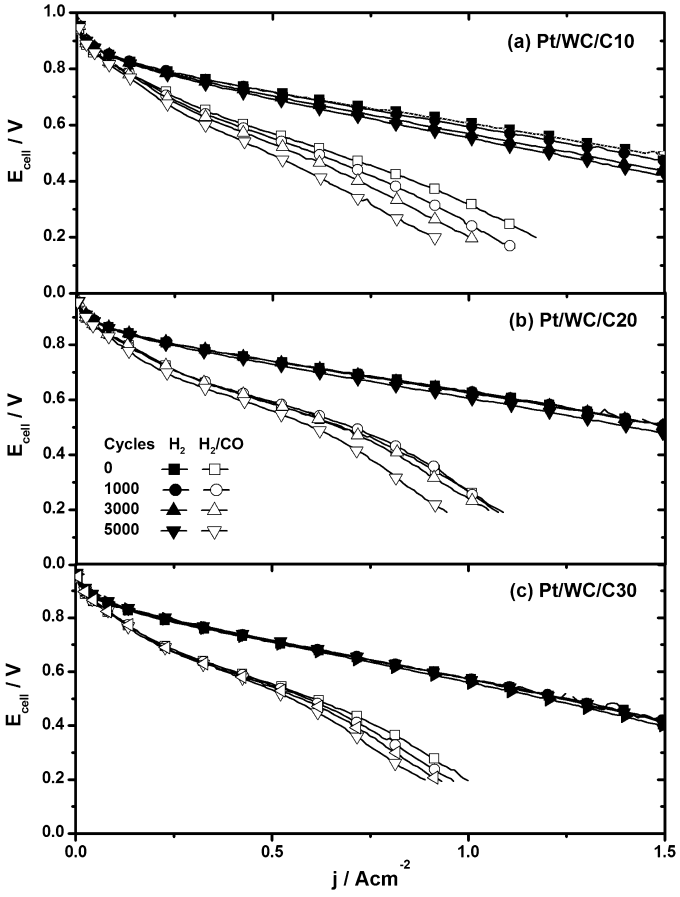

Fig. 4. PEM single cell polarization curves measured at 85 °C. The anodes Pt/WC/C10 (a), Pt/WC/C20 (b) and Pt/WC/C30 (c) were supplied with pure H_2 and H_2/100 ppm CO and the Pt/C cathodes were supplied with O_2.

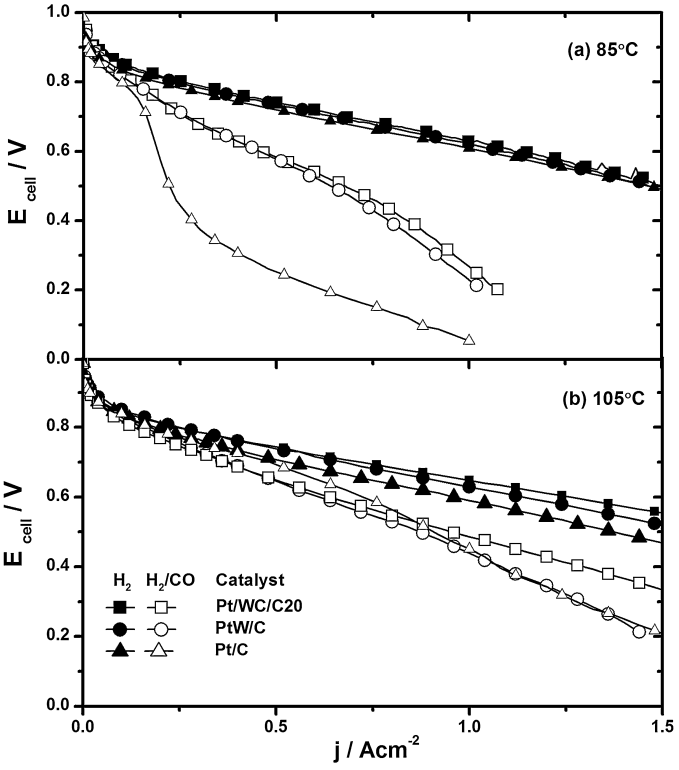

Fig. 5. PEM single cell polarization curves measured at 85 °C (a) and 105 °C (b). The Pt/WC/C20 and PtW/C anodes were supplied with pure H_2 and H_2/100 ppm CO and the Pt/C cathodes were supplied with O_2.

also a contribution toward CO oxidation by the carbide phase. It has been investigated that the bonding between CO and tungsten carbides is much weaker than the bonding between CO and Pt, thus rendering the tungsten carbide catalyst sufficient immunity against CO poisoning [20]. Furthermore, it has been shown that WC can easily activate water to form surface hydroxyl [11]. The oxidation of adsorbed CO on Pt surface in the presence of WC proceeds through the following reaction [23].

$$\text{Pt—CO} + \text{WC—OH} \rightarrow \text{Pt} + \text{CO}_2 + \text{WC} + \text{H}^+ + \text{e}^- \quad (1)$$

Bernett et al. [33] has reported that WC alone is immune to CO poisoning in the presence of H_2, although the effect is not as efficient for Pt/WC. However, the CO poisoning of Pt cannot be avoided completely, because of its participation in reaction along with WC. Besides, as the concentration of W in Pt/WC/C20 is greater than that in PtW/C, the higher CO tolerance of the former could also be attributed to higher content of W, as shown previously [31].

Further insights into these issues were possible from online mass spectrometry (OLMS) measurements with CO_2 detection, while keeping the cell under the operating conditions of increasing current densities at two different temperatures. Fig. 6 shows plots of the anode overpotential and the CO_2 production as a function of current density at two different cell temperatures for Pt/WC/C20, PtW/C and Pt/C catalysts. These results clearly confirm that the increase of the cell temperature enhances the anode performance (or reduces the overpotentials) with H_2 containing 100 ppm of CO, for the three catalysts. It can be clearly observed from Fig. 6 that the CO_2 production increases distinctively with the increase in temperature for all the catalysts, however in the case of PtW/C and Pt/C, the

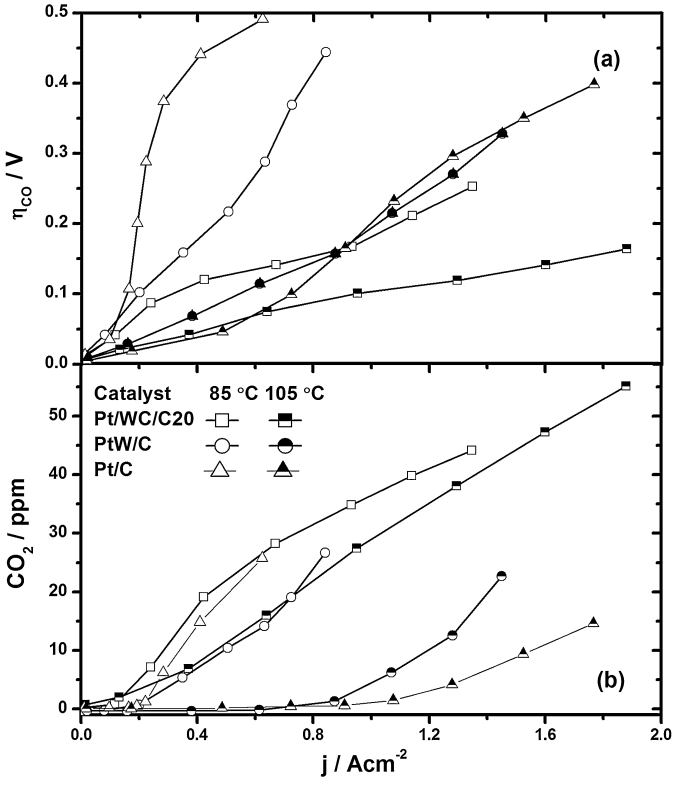

Fig. 6. Anode overpotential due to the presence of CO (η_{CO}) vs. current density (a) and CO_2 production vs. current density obtained by OLMS (b) plots for single cell with the anodes formed by Pt/WC/C20 and PtW/C catalysts at 85 and 105 °C.

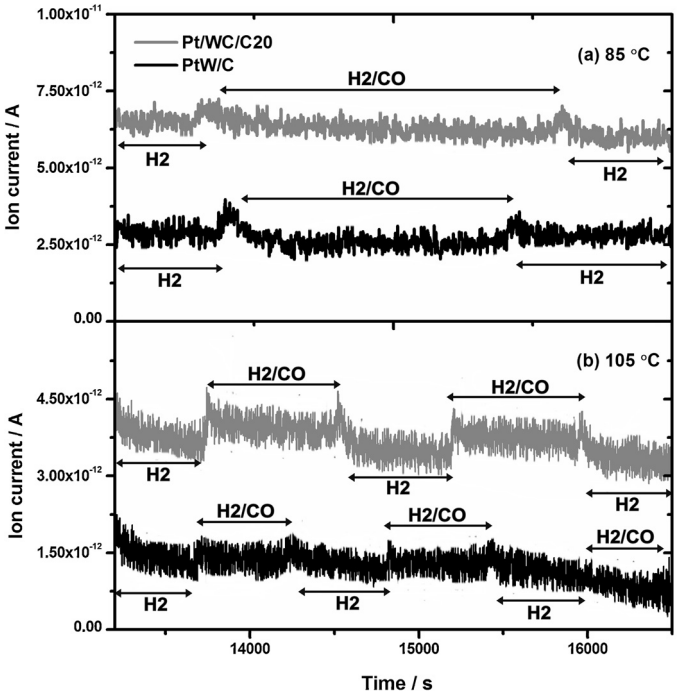

Fig. 7. Ion current with m/z= 44 detection obtained by OLMS for the Pt/WC/C20 and PtW/C anodes, supplied with H_2 or H_2/100 ppm CO. Cathodes formed by Pt/C and supplied with O_2.

CO_2 production is much lower than for Pt/WC/C20 at the two temperatures. This explains the better CO tolerance of the carbide based catalyst as compared to the bimetallic catalyst. One more observation deduced from Fig. 6 is that, as the CO_2 production increases, the anode overpotential generally decreases and vice versa.

Fig. 7 shows the results of OLMS experiments in which the cell was kept at open circuit and the anode was first fueled with pure H_2 and then switched to H_2/100 ppm CO, repeating the process several times, while the cathode was constantly fed with O_2. It can be observed that at 85 °C (see Fig. 6a), CO_2 production is almost zero when the anode is fed with H_2/100 ppm CO for both the Pt/WC/C20 and PtW/C electrocatalysts. When the temperature is increased to 105 °C, as shown in Fig. 7b, CO_2 production occurs when Pt/WC/C20 electrocatalyst is exposed to H_2/CO, which clearly indicates the occurrence of CO oxidation on the surface of electrocatalyst possibly through the water gas shift reaction [7]

$$CO_{ads} + H_2O \rightarrow CO_2 + H_2 \quad (2)$$

and/or by oxygen crossover from the cathode, whereas for PtW/C no oxidation takes place. Although the extent of this process is much smaller than for Pt–Mo-based materials, results in Fig. 7 show that at higher temperature the tungsten carbide-based electrocatalyst is more effective for the CO oxidation than the PtW/C electrocatalyst. These results are consistent with the polarization curves, which showed a greater CO tolerance for Pt/WC/C20 anode.

In order to evaluate the surface properties, cyclic voltammetry of anode electrocatalysts was conducted at room temperature and the results are shown in Fig. 8. All the cyclic voltammograms show the typical Pt features for the underpotential (UPD) adsorption/desorption of hydrogen (0.05 to 0.35 V vs RHE). Beyond the UPD region the peaks in the 0.35–0.45 V vs. RHE range can be observed in the cyclic volatammograms of all electrocatalysts except Pt, which are mainly related to the redox processes involving tungsten [31,34]. However, the double layer region in PtW/C is broader than in Pt/WC/C20, probably due to the presence of tungsten oxygenated species [34].

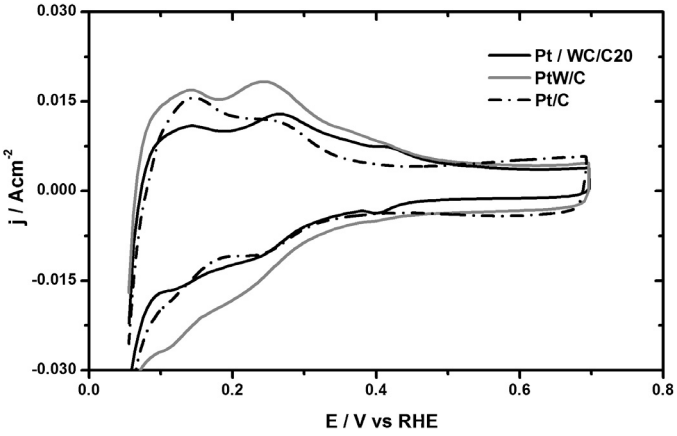

Fig. 8. Cyclic voltammograms of Pt/WC/C20 (a) PtW/C (b) anodes.

The CO stripping profiles together with the CO_2 mass signal detected by OLMS are shown in Fig. 9 for three catalysts at different temperatures. Results show that, an increase in temperature induces a decrease of the CO oxidation potential and the CO coverage for both catalysts. As shown before, this reduction of the CO coverage is responsible for the increase of the current densities with the increase of temperature (see Fig. 6). For the Pt/WC/C20 the CO oxidation occurs at lower potentials at all temperatures as compared to PtW/C and Pt/C, which is in agreement with a relatively greater CO tolerance of the carbide based electrocatalyst. Thus the better CO tolerance of Pt/WC/C20 as compared to PtW/C was not only shown by polarization curves and online mass spectrometry experiments, but also by CO stripping experiments. The CO stripping potentials for Pt/C occur at almost the same values as for PtW/C, which are consistent to polarization curves where nearly the same CO tolerance was shown by Pt/C to PW/C, particularly at higher temperature.

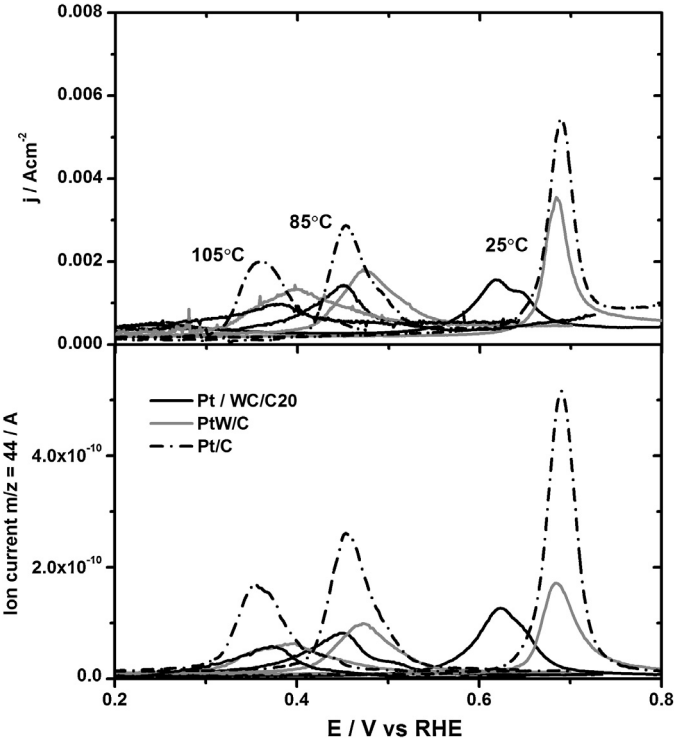

Fig. 9. CO stripping curves (a) and CO_2 production measured by OLMS (b) for the anodes formed by Pt/WC/C20 and PtW/C electrocatalysts at 25, 85 and 105 °C.

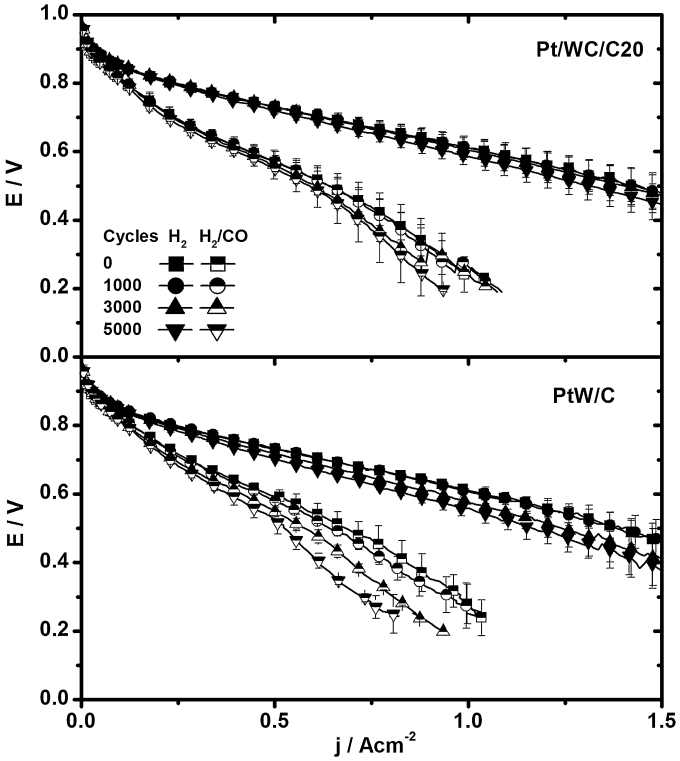

Fig. 10. PEM single cell polarization curves measured with freshly prepared electrodes, after 1000, 3000 and 5000 potential cycles. The Pt/WC/C20 (a) and PtW/C (b) anodes were supplied with pure H_2 and H_2/100 ppm CO and the Pt/C cathodes were supplied with O_2.

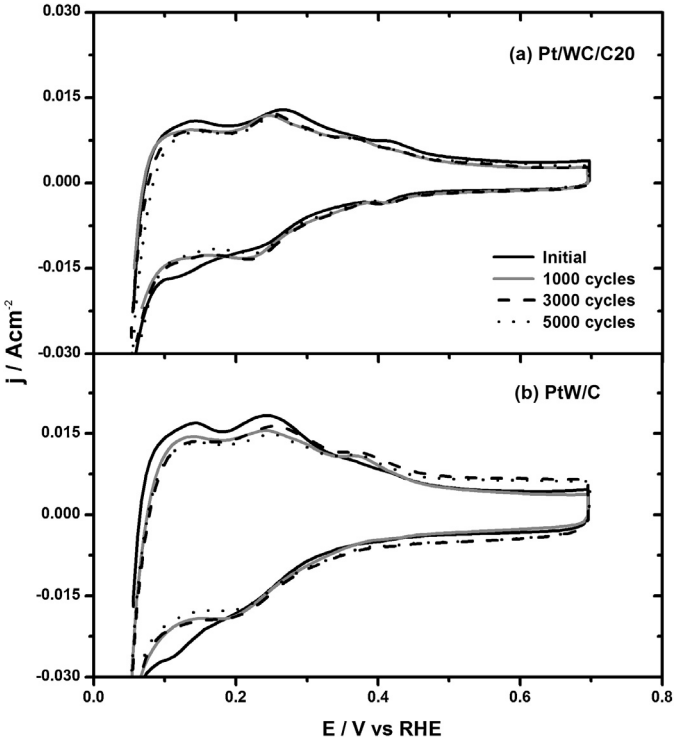

Fig. 11. Cyclic voltammograms of anodes composed of Pt/WC/C20 (a) PtW/C (b) anodes, measured after initial polarization measurement, after 1000, 3000 and 5000 voltage cycles.

3.3. Stability of the electrocatalysts

Fig. 10 shows the polarization curves for the Pt/WC/C20 and PtW/C catalyst which were recorded initially with freshly prepared electrodes and then after various stages of the cycling process. While the cell voltage remains practically constant in the presence of H_2 and decreases slightly in the presence of H_2/CO for the Pt/WC/C20 (Fig. 10a), a continuous decrease in cell voltage is observed in the presence of H_2 as well as H_2 containing 100 ppm of CO for the PtW/C20 (Fig. 10b) and Pt/WC/C10 (Fig. 3a) catalysts. A constant behavior in performance is also shown by Pt/WC/C30 (Fig. 3c). These results show that the Pt/WC/C catalysts with WC percentages above 20% are more stable than PtW/C when operating in the PEM single cell anode. For Pt/C quite constant performance up to 5000 voltage cycles was observed in the presence of both H_2 and H_2 containing 100 ppm of CO and can be seen in our work previously published [35].

In order to further compare the stability of the electrocatalysts, cyclic voltammograms were recorded initially after the first polarization measurements and then after 1000, 3000 and 5000 cycles, as shown in Fig. 11 for the Pt/WC/C20 and PtW/C catalysts. A practically constant behavior is observed either for Pt/WC/C20 or for PtW/C, because constant current densities and fix positions of the oxidation/reduction peaks are noted after 1000 cycles. On the other hand for the PtW/C, the double layer currents increase, possibly indicating the formation of surface oxides. In this way, the higher stability of the Pt/WC/C20 electrocatalyt is not only shown by polarization curves and anode overpotentials (see Fig. S2 in the supporting material), but also by the cyclic voltammograms of the anodes. The little greater stability of Pt/WC/C electrocatalysts is most probably due to its carbide phase which is more corrosion resistant in acidic medium, as compared to the carbon or tungsten present in the bimetallic PtW/C electrocatalyst, as shown by the appearance of WO_3 peaks in XRD pattern (see Fig. 12) of the PtW/C catalysts after testing in the fuel cell, whereas in the case of Pt/WC/C20 no such peaks appeared. It has been reported that WO_3 react with H_2 to produce hydrogen tungsten bronze (H_xWO_3), which is soluble in water [36]. Thus the degradation in performance is most likely due to the formation of these oxide species which leads to the slow formation of hydrogen tungsten bronze and finally to the detachment of Pt particles from the surface of the electrocatalysts after dissolution of the bronze. Similar results have been reported previously [37]. The effect of potential cycling on the particle size of the electrocatalysts was investigated by TEM and the results obtained are shown in Fig. 13. As can be seen from the values given in the Table 1, the particle size of Pt/WC/C20 catalyst practically remains constant after testing in the fuel cell, although a small agglomeration of particles was observed for this catalyst. On the other hand a small increase in the particle size was observed for

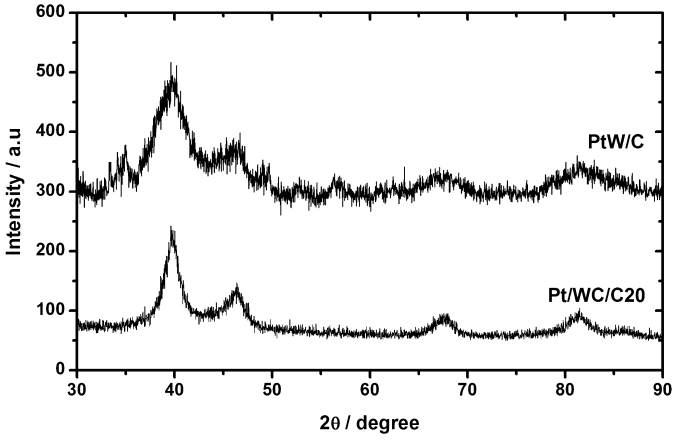

Fig. 12. XRD patterns of Pt/WC/C20 and PtW/C catalysts after testing.

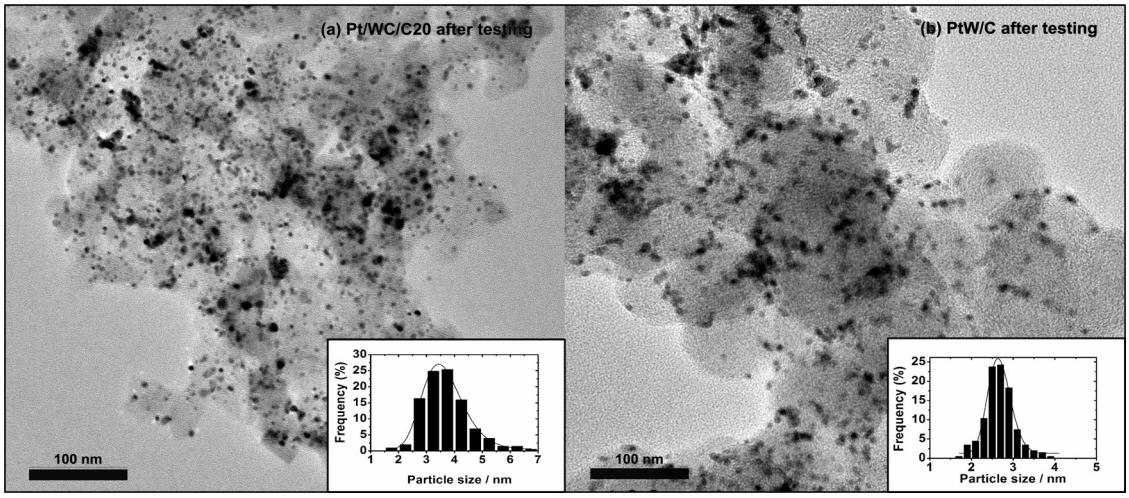

Fig. 13. TEM images of Pt/WC/C20 (a) and PtW/C (b) catalysts after testing.

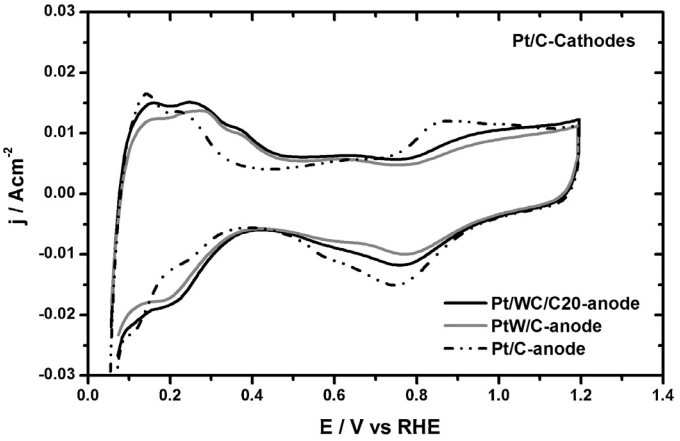

Fig. 14. Cyclic voltammograms of the Pt/C cathodes measured after 5000 potential cycles of the Pt/WC/C20 and PtW/C anodes.

the PtW/C, as shown in Table 1. Thus here also, a greater stability was shown by the Pt/WC/C20 as compared to PtW/C catalyst.

The extent of W dissolution from the anode electrocatalysts was confirmed by the cyclic voltammetry of Pt/C cathodes after 5000 potential cycles, as shown in Fig. 14. The peaks present in the potential range of 0.35–0.45 V vs. RHE, except for Pt/C, are exactly the same as in the voltammetric profiles of the anodes. Thus, it is certain that a portion of W dissolved from the anode, travelled through the electrolyte membrane and reached the cathode. This crossover of the W species may be other factor responsible for the decline in the CO tolerance of single cell anodes. Similar fact has also been observed previously for PtMo/C and PtRu/C electrocatalyst, where the Pt cathode was contaminated by the Mo and Ru species after polarization measurements [6,7]. As in these cases, the decay of the cell performance in the absence of CO is most probably due to the influence of W contaminants on the activity of oxygen reduction reaction, but the effect produced by the Mo [8] is much more adverse than that produced here by W.

4. Conclusions

WC/C has been synthesized by a simple impregnation method and characterized physically by XRD, EDS and TEM and electrochemically by polarization curves, cyclic voltammetry, online mass spectrometry and CO stripping experiments. Pt supported on this material has shown a higher activity for electrochemical oxidation of hydrogen with and without CO than a PtW/C catalyst. As catalyst support, WC/C showed to be somewhat more stable against oxidation than Vulcan XC-72 carbon, as evidenced by potential cycling experiments. Cyclic voltammetry of cathodes has shown that partial dissolution of W occurs from the anodes electrocatalysts due to acidic environment of fuel cell. Since the Pt/WC/C20 is reasonably stable in electrochemical environment and significant tolerant to CO at higher temperature, it could become an alternative catalyst for PEMFC to replace the carbon-dispersed Pt–Ru and Pt–Mo electorcatalysts.

Acknowledgments

The authors would like to thank the Third World Academy of Science (TWAS), Italy, the Conselho Nacional de Desenvolvimento Científico e Tecnológico (CNPq), and Fundação de Amparo a Pesquisa do Estado de São Paulo (FAPESP - Proc. 2013/16930-7), Brazil, for financial supports.

Appendix A. Supplementary data

Supplementary data associated with this article can be found, in the online version, at http://dx.doi.org/10.1016/j.apcatb.2014.10.068.

References

[1] V.S. Bagotsky, Fuel Cells-Problems and Solutions, second ed., John Wiley & Sons, Inc. Publication, Canada, 2012, pp. 43–69.
[2] A. Rabis, P. Rodriguez, T.J. Schmidt, J. Am. Chem. Soc. Catal. 2 (2012) 864–890.
[3] J.J. Baschuk, X. Li, Int. J. Energy Res. 25 (2001) 695–712.
[4] F. Hajbolouri, B. Andreaus, G.G. Scherer, A. Wokaun, Fuel Cells 4 (2004) 160–168.
[5] S. Ball, A. Hodgkinson, G. Hoogers, S. Maniguet, D. Thompsett, B. Wong, Electrochem. Solid-State Lett. 5 (2002) A31–A34.
[6] E. Antolini, J. Solid State Electrochem. 15 (2011) 455–472.
[7] T.C.M. Nepel, P.P. Lopes, V.A. Paganin, E.A. Ticianelli, Electrochim. Acta 88 (2013) 217–224.
[8] A. Hassan, A. Carreras, J. Trincavelli, E.A. Ticianelli, J. Power Sources 247 (2014) 712–720.
[9] L. Nikolov, T. Vitanov, V. Nikolova, J. Power Sources 5 (1980) 197–206.
[10] R. Venkataraman, H.R. Kunz, J.M.J. Fenton, J. Electrochem. Soc. 150 (2003) A278–A284.
[11] M.B. Zellner, J.G. Chen, Catal. Today 99 (2005) 299–307.
[12] F.P. Hu, P.K. Shen, J. Power Sources 173 (2007) 877–881.
[13] G. Lu, J.S. Cooper, P.J. McGinn, J. Power Sources 161 (2006) 106–114.
[14] H. Meng, P.K. Shen, J. Phys. Chem. B 109 (2005) 22705–22709.
[15] H. Chhina, S. Campbell, O. Kesler, J. Power Sources 179 (2008) 50–59.
[16] R. Ganesan, D.J. Ham, J.S. Lee, Electrochem. Commun. 9 (2007) 2576–2579.
[17] K. Lee, A. Ishihara, S. Mitsushima, N. Kamiya, K. Ota, Electrochim. Acta 49 (2004) 3479–3485.

[18] J.S. Moon, Y.W. Lee, S.B. Han, K.W. Park, Int. J. Hydrogen Energy 39 (2014) 7798–7804.
[19] D.R. McIntyre, G.T. Burstein, A. Vossen, J. Power Sources 107 (2002) 67–73.
[20] X.G. Yang, C.Y. Wang, Appl. Phys. Lett. 86 (2005) 224104–1224104.
[21] H. Wu, J.G. Chen, J. Vac. Sci. Technol. A 21 (2003) 1488–1493.
[22] R. Ganesan, J.S. Lee, Angew. Chem. Int. Ed. 44 (2005) 6557–6560.
[23] D.J. Ham, Y.K. Kim, S.H. Han, J.S. Lee, Catal. Today 132 (2008) 117–122.
[24] T.G. Kelly, S.T. Hunt, D.V. Esposito, J.G. Chen, Int. J. Hydrogen Energy 38 (2013) 5638–5644.
[25] Y. Liu, W.E. Mustain, Int. J. Hydrogen Energy 37 (2012) 8929–8938.
[26] S. Zhang, X.Z. Yuan, J.N.C. Hin, H. Wang, K.A. Friedrich, M. Schulze, J. Power Sources 194 (2009) 588–600.
[27] J.B. Joo, J.S. Kim, P. Kim, J. Yi, Mater. Lett. 62 (2008) 3497–3499.
[28] E.I. Santiago, G.A. Camara, E.A. Ticianelli, Electrochim. Acta 48 (2003) 3527–3534.
[29] V. Radmilovic, H.A. Gasteiger, P.N. Rose, J. Catal. 154 (1995) 98–106.
[30] E.I. Santiago, M.S. Batista, E.M. Assaf, E.A. Ticianelli, J. Electrochem. Soc. 151 (2004) A944–A949.
[31] L.G.S. Pereira, F.R. Santos, M.E. Pereira, V.A. Paganin, E.A. Ticianelli, Electrochim. Acta 51 (2006) 406–4066.
[32] A.K. Shukla, M.K. Ravikumar, A.S. Arico, G. Candiano, V. Antonucci, N. Giordano, A. Hamnett, J. Appl. Electrochem. 25 (1995) 528–532.
[33] C.J. Barnett, G.T. Burstein, A.R.J. Kucernak, K.R. Williams, Electrochim. Acta 42 (1997) 2381–2388.
[34] Y. Dai, Y. Liu, S. Chen, Electrochim. Acta 89 (2013) 744–748.
[35] A. Hassan, V.A. Paganin, A. Carreras, E.A. Ticianelli, Electrochim. Acta 142 (2014) 307–316.
[36] M. Zayat, R. Reisfeld, H. Minti, B. Orel, F. Svegl, J. Sol-Gel Sci. Technol. 11 (1998) 16–168.
[37] H. Chhina, S. Campbell, O. Kesler, J. Power Sources 164 (2007) 43–440.